Chapter 1 Introduction

1.1. Color Changing Materials

Compounds that change color visibly and reversibly when subjected to a change in their environment (heat, light, pressure, electrons, etc.), are known as chromogenic materials. There are four major categories – electrochromic (EC), thermochromic (TC), photochromic (PC) and piezochromic (PEC). The change in optical properties can be in the form of absorption, reflectance, or scattering. The change can be either within the visible, or beyond visible spectrum. Chromogenesis is one of the most exciting, but also complex research topics. The two major types are the nonelectrically activated and electrically activated types. The non-electrically activated type includes photochromics, and thermochromics [1].

Thermochromic (TC) Materials. They change reversibly color with changes in temperature (Fig. 1-1). They can be semi-conductor compounds, liquid crystals or metal compounds. Thermochromic materials change color by a process which involved a thermally induced chemical reaction or a phase transformation. The change in color happens at a determined temperature, which can be varied by doping the material. Thermochromism is seen in a large number of organic and certain inorganic compounds. Organic compounds such as anil, spiropyrans, polyvinyl acetal resins, and hydroxide groups readily exhibit thermochromism. Inorganic TC compounds include AgI, Ag_2HgI_4, HgI, HgI_2, $SrTiO_3$, along with several cobalt, copper and tin complexes. They can be used to make paints, inks or are mixed to molding or casting materials for different applications [2]. The reported examples of TC solids involve color changes due to changes of stereochemistry. Salts of mercuric iodide, M_2HgI_4 [M= Cu (I), Ag(I)] are easily prepared and exhibit sharp, reversible TC transitions at moderately low temperatures. The Ag(I) solid changes color from yellow to orange at 50 °C and the Cu(I) solid at 67 °C. The color changes are due to changes in crystal structure [3]. VO_2 is a well known TC material too. The TC process can occur through replacement of some of the vanadium by other metals or oxygen.

There is another kind of material - Thermotropic (TT) Materials which can also be classified as TC materials. The phase change in a thermotropic material can cause a significant change in its electronic properties from an insulator to semiconductor

transition or from a semiconductor to metallic state when a “critical” temperature is exceeded. Some of these compounds are Fe_3O_4, NbO_2, NiS, Ti_2O_3 and VO_2[4]. Vanadium dioxide, VO_2 has also been considered for window applications [5]. By substitutional doping of vanadium in VO_2, an improvement on the transformation temperature can be achieved. They return to their original condition when they go back to the starting temperature. Some materials exhibit hysteresis during their heating and cooling cycle. In the Chapter 8 more details are shown concerning V_2O_5 films (as TC and TT) deposited within the frame of this study.

Fig. 1-1. Thermochromic materials change reversibly color when they are heated or cooled.

Photochromic (PC) Materials. They change material state from transparence to color when they are exposed to light, and revert to transparency when the light is dimmed or blocked. The change of PC material is one of the oldest phenomena in switching and dates back to the 1880s. Generally PC materials are energy absorptive. Basically the physical phenomenon involved is the reversible change of a single chemical species between two energy states that have different absorption spectra. The changes in states can be induced by electromagnetic radiation, usually UV light. PC materials have potential in advanced glazing. The main application is in the field of sunglasses. To become photochromic a special glass containing metal halides such as AgCl or AgBr is made. A special heat treatment of this composition causes the formation of photosensitive silver halide crystals with 15 nm in size. When UV light of the wavelength between 300-400 nm illuminates the glass, the metal halide crystals disassociate into metallic silver and the halide. The effect causes visible absorption

takes place. When the UV light is removed, the metal-halide molecule recombines thermally to its original form and as a result the glass becomes more transparent. Photochromic lenses automatically lighten and darken depending on changing daylight conditions, even behind a windshield [6].

1.2. Electrochromic (EC) Materials

Until now EC materials have been finding several applications like in smart windows (or EC windows, Fig. 1-2), anti-dazzling rear view mirrors, switchable motorcycle helmet (Fig. 1-3), for contrast-enhancement in some emissive display devices and in non-emissive large-area color display for information advertisement [7-11]. The smart windows are of great interest for special fields in architectural glazing of building and sunroof of automotive. Furthermore, they have no moving parts and the maintenance costs are minimal. The absorption or reflection of light in the visible and near infrared region can be adjusted according to the environment with an applied electric field or voltage (~5 V). In other words they are able to turn a transparent glazing into a color tinted glazing and then turn it back again. Thus a dynamic control of solar energy radiation and infrared radiation can significantly lower the air conditioned energy consumption in hot summer and cold winter.

Fig. 1-2. South facing view of a portion of the 8 x 17 m electrochromic E-Control™ glass made by Flabeg and installed in the Stadtsparkasse Dresden am Altmarkt. The left portion of the window is colored. (Source: H. Wittkopf, Flabeg.) [11].

The study of electrochromic materials is an interdisciplinary field. In an electrochemical cell of EC devices (ECDs) the discharged positive ions (guest atoms)

are free to diffuse in a thin solid film (electrode) of host material, modifying its electronic structure to create a colored material. The change is also thought as an oxidation-reduction reaction in chemistry, using either inorganic or organic compounds, and the color change can occur at either the anode or the cathode thin film. There are two major class materials, the ion-insertion/extraction type such as tungsten trioxide, and the non-insertion group such as the viologens.

Fig. 1-3 Switchable motorcycle helmet visor made by ChromoGenics. Shown are two colorations of the visor (Credit: C. Granqvist, ChromoGenics.) [11].

Tungsten Trioxide (WO_3). The WO_3 is ubiquitous and one of the best choices for the primary working electrode material in ECDs. It is common one as an active EC layer for potential application in advanced glazing and large area displays [7, 8]. The WO_3 is one of the best EC performances due to its high charge capacity and long-term cyclability. It goes blue on insertion of Li, or other metal, hydrogen and guest atoms. More details are presented in Chapter 7 and Chapter 10.

Viologens. Viologens are family of halides of quaternary bases derived from 4,4'-bipyridinium. One viologen example is 1, 1'-diheptyl-4,4'-bipyridinium bromide, which changes from clear to bluish purple. The most common application of viologen has been the electrochromic interior rearview mirror available for car. It utilizes a substituted viologen as the cathode coloring material, with a compound like phenylene diamine as the anode colouring electrochromic material.

Other Materials. In fact numerous inorganic, some organic and polymer EC materials have been discovered and studied. Inorganic EC materials are especially important in technology because of their highly stable properties, potential and wide applications [12-14]. So far, much effort has been focused on transition metal oxides based

on tungsten (W) [15], molybdenum (Mo) [16], vanadium (V) [17], titanium (Ti), iridium (Ir), and nickel (Ni) [18-20]. Recently Wang et al [21] reported that Rhodium oxide (Rh_2O_3) films prepared by sol-gel method exhibit reversible electrochromic behavior. The Rh_2O_3 film on anodic electrode in alkaline solution (1 M NaOH) presents a color change between lemon yellow (reduced state of Rh_2O_3-$5H_2O$) and olive green (oxidation state of RhO_2-$2H_2O$).

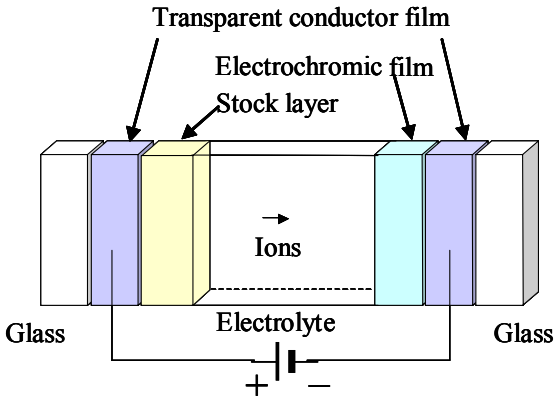

Fig.1-4. A basic electrochromic film device structure.

1.3. Structure of the EC Windows

A basic smart window structure of electrochromic (EC) film is proposed in Fig.1-2. The micrometer-thick multi-layer structure contains two transparent electrical conduction layers and two electrodes capable of charge (ion) insertion/extraction. One of the electrodes must be electrochromic; usually it consists of tungsten oxide. The other, i.e., the counter electrode (CE), can either be a complementary coloring EC material or a material remaining transparent upon charge insertion (call it stock layer or ion storage layer). The lack of a suitable counter electrode has been an obstacle for development of the high quality EC devices. As we know the WO_3 and other EC devices require a counter electrode or ion storage (IS) such as Nb_2O_5 , V_2O_5 , NiO and IrO_2 which can supply Li (or H), but remains colourless or complementary color in the process. In the literature there are some typical configurations of ECDs described as following.

ITO/NiO_xH_y /WO_3 / ZrO_2 (or ZrP-electrolyte)/WO_3 /ITO configuration [22]**:** C. G. Granqvist et al reported a six-layer device which was made by reactive dc magnetron sputtering. In the structure the electrochromic layer is WO_3. The layer for ion storage is nickel oxide (NiO) film or others. The WO_3 between the acidic ZrO_2 (or ZrP-based

electrolyte) and the NiO_xH_y film served as optically passive protective layer. The optical inactivity of the protective layer could be understood from arguments based on electron density of states. A transparent conductor-ITO (indium tin oxide) serves as the electrical bottom contact.

ITO /WO_3 / porous ZrO_2 / $GdMgH_y$ /dense ZrO_2 /ITO configuration: A forward step in technology was made by Van der Sluis et al. They alloyed gadolinium (Gd) with magnesium (Mg), and reached a color neutral transparent state in the switch mirrors [23]. The all-solid state device consists mainly of 5 different square-shaped thin films, sputter-deposited on a transparent substrate. A GdMg alloy and a porous ZrO_2 electrolyte were deposited on the WO_3 hydrogen storage layer. The alloy is loaded with hydrogen during sputtering and is therefore transparent directly after deposition. The resistivity of this alloy is low enough so that the layer can be used as an electrical top-contact. To avoid hydrogen escape, a dense ZrO_2 layer is deposited on top of the stack.

[ZnS/Ag/ZnS] / WO_3 / $Li^+V_2O_5$/ [ZnS/Ag/ZnS] configuration: The thin film layers were prepared by thermal evaporation and electron gun deposition [24, 25]. The WO_3 films (thickness: 300 nm to 600 nm) were used as active EC layers and textured WO_3 film were also developed. The structure allows Li^+ intercalation deeper into the oxide matrix, thus doubling the diffusion coefficient. The ECDs were fabricated with optimized ZnS/Ag/ZnS coatings as transparent conductors. The use of multilayer ZnS/Ag/ZnS film was found to improve the electrical characteristics and to lower the emittance of the devices. V_2O_5 ion storage thin films were Li^+ doped both electrochemically and in vacuum leading to a 20% increase of the EC device coloration efficiency.

There are also other kinds of structures like **ITO/WO_3 /electrolyte/ZrO_2 /NiOx /ITO configuration**[26] (Polymer electrolytes were used in this electrochromic device, see section 1.4.3) and **FTO** (Tin oxide doped fluorine) **/Nb_2O_5/electrolyte/TiO_2 - CeO_2 /FTO configuration**[27] (Niobium pentoxide **(**Nb_2O_5) is cathodic EC material).

1.4. Smart Windows Development

Commercial interest in ECDs has led to the development of many different structures and types as theories described above. In the following sect some of the developed styles and novel concepts of ECDs are presented for future applications.

1.4.1. Complementary electrochromic structure

Complementary EC devices have advantages in offering deeper switching over singer-EC layer devices. Complementary materials to WO_3 include iridium oxide, nickel hydroxide, Prussian blue (PB), polyaniline and its derivatives. When an adequate voltage is applied between WO_3 and one of these complementary electrodes, such that the WO_3 electrode is the cathode and the complementary electrode is the anode, both films color simultaneously. WO_3 is called a cathodically coloring material and its complementary counter part is an anodically coloring one. The tungsten oxide - prussian blue (PB) system is a typical solid state on EC configuration of H_xWO_3/H^+-SPE/PB [28].

It is important to gain an insight into the dominant factors that control the electrochromic performance. In future studies, the design of complementary ECDs with two reversible redox electrodes operating in series can be presented. By combining the electrochemical and optical properties of these two electrodes, design equations suitable for complementary ECDs can be derived [28]. After overall extent and electrodes with the least charge capacity is valued, the effect of charge (ion) capacity ratio on the optical attenuation range can be predicted. The required operational parameters in the design equations can be evaluated from the fabricated cell.

1.4.2. Flexible electrochromic devices

Building the EC device on a flexible substrate appears to be very interesting since such a device could be fabricated in varying shapes. Substrates can be chosen among the commercially available products: polyethylene terephtalate (PET) covered with an ITO-coating. The deposition of WO_3 and other films can be made onto ITO/PET by sol-gel, magnetron sputtering and other methods. The electrochromic properties of these films have been analyzed in a three-electrode cell with 1 M $LiClO_4$/propylene carbonate electrolyte. The flexible EC device with micro-porous membrane metallized with gold that acts both as an electrode and a reflecting layer is a kind of selection [29-31]. In the NANOEFFECT[31] project of our group, electrochromic smart plastic devices, with the nanocomposites and high colouration efficiency, will be also developed.

1.4.3. Polymer electrolytes for EC devices

Generally polymers can be used in proposed electrochromic devices as EC material, electrolyte solution thickeners, the matrix of electrolyte gels, solid polymer electrolytes, semipermeable membranes and sealants. Each type of application of polymers has its potentiality in ECDs.

As we know one of the absolutely central problems related with ECDs is associated with the electrolyte and its stability. Polymer composite electrolytes have been under extensive investigation for applications in ECDs. These investigations were mainly concerned with lithium salts dissolved in PMMA (or other type polymers) and various added solvents (plastersizers). Whether this becomes a gel or remains as liquid is an open question [14]. Proton conducting polymer complexes with inorganic acids (H_2SO_4, H_3PO_4) show excellent electrical and optical properties. Their high chemical activity is, however, a drawback for practical applications. It has been shown [32] that the electrical conductivity (10^{-3} -10^{-4} S/cm at room temperature) and optical properties of inorganic oxide particle hydrate (antimonic acid, aluminum oxide, SiO_2) nanocomposites with polyvinyl acetate are suitable for electrochromic applications. The chemical activity and hygroscopicity of the nanocomposites are lower than the corresponding properties of acid-based electrolytes. Polymer electrolytes were tested in ECDs designed according to the system-glass substrate /ITO/WO_3/electrolyte/ZrO_2/NiOx/ITO/ glass substrate[26]. The transmittance of electrolyte layers with the thickness up to 200 mm is sufficiently high for use in ECDs. For the thicker layers, scattering by particles reduces the transmittance of the composite layer.

1.4.4. Non-conjugated EC polymers derived from aromatic amine derivatives

Electrically conducting polymers, such as polythiophene, polypyrrole, polyaniline, and their derivatives, have generated a large amount of interest in the field of electrochromic materials. The electrically conducting polymers have a disadvantage for the window application since the undoped states of the polymers are colored because of their long conjugation lengths. Y. Nishikitani *et al* [29] reported the EC properties of a non-conjugated polymer synthesized by condensation polymerization of an aldehyde and an aromatic amine derivative, which is colorless transparent in its undoped state and dark yellow, when oxidatively doped. The polymer DDP-AA was synthesized by the polymerization of acetaldehyde (AA) and N,N'-dimethly-N,N'-diphenyl-1,4-phenylenediamine (DDP). DDP-AA is soluble in polar solvents like chloroform and can be cast on an ITO substrate to form thin film. The cyclic voltamogram (CV) of the film showed two reversible redox couples producing mono-oxidised and di-oxidised DDP-AA states. The colors of these EC states are, respectively, blue and purple.

1.4.5. Photovoltaic powered and gas sensitive smart windows

Multi-functional smart windows have also shown the attractive application in daily life. One is the integrated PV (photovoltaic) powered EC window (or combined PV and EC window) [33]. Another is EC window or EC device with sensor such as gas detection for both building and instrument systems. We studied the bi-layer CdS (cadmium sulfide)/ITO film for former style - PV powered ECDs in Chapter 6. The CdS /ITO film is used to link PV and EC part and acts as one of functional layers. The SnO_2 film can be investigated to form counter electrode layer as ion storage function in the EC windows and to form a film sensor as gas sensitive function in the EC windows.

1.5. Summary of the Chapter and Research Content of the Thesis

Summaries of the color-changing materials, EC materials and different ECDs configurations are given. Some quintessential and developing ECDs such as complementary electrode, flexible devices, advanced transparent electrode and polymers devices are introduced.

Based on the above introduction, components contents of the thesis include investigations of transparent conduction films, electrochromic films, counter electrodes films, and multi-layer structures. Multilayer films based on tungsten oxide (WO_3) are mainly deposited by reactive dc magnetron sputtering onto glass substrates for EC application. The configuration of our smart window is chosen as ITO/WO_3/Li^+-electrolyte/counter electrode film/ITO. It is all solid state ECDs for future application. Depending on the choice of different counter electrodes such as SnO_2, V_2O_5, ZrO_2 and the relevant doped Mo (or Fe) films, different window structures are fabricated and studied. The ITO, WO_3, ZrO_2 and V_2O_5 films are characterized by X-ray diffraction (XRD), X-ray photoelectron spectroscopy (XPS), energy dispersive X-ray (EDX), scanning electron microscopy (SEM) and atomic force microscopy (AFM). Some of the films are also analyzed in the range of mid infrared, near infrared, visible-ultraviolet spectral regions. The transmission, absorption, and reflection spectrum techniques are used.

1.5. References

[1] Granqvist, C.-G., Handbook of Inorganic Electrochromic Materials, Elsevier, Amsterdam, (1995)

[2] J. H. Day, "Chromogenic materials," in Ency. of Chemical Technology, J. Wiley, NY (1977); K. Sone and Y. Fukuda, Inorganic Thermochromism. Springer, Berlin, Germany (1987).

[3] Hughes, Jeffrey G. Thermochromic Solids J. Chem. Educ., (75) (1998) 57.

[4] D. Adler, "Thermochromic Compounds" Rev. Mod.Phys.40 (1968) 714.

[5] S. M. Babulanam, T. S. Eriksson, G. A. Niklasson, and C. G. Granqvist, "Thermochromic V02 films for energy efficient windows," Solar Energy Mat. 16 (1987) 347.

[6] R. J. Araujo, "Opthalmic glass particularly photochrom. glass," Non-Cryst. Solids 47 (1982) 69.

[7] C. G. Granqvist, Electrochimica Acta 44 (1999) 3005.

[8] G. Leftheriotis, S. Papaefthimiou, P.Yianoulis, Sol. Energy Mater. Sol. Cells, 61 (2000) 107.

[9] Lars Berggren, Gunnar A. Niklasson, Optical absorption and durability of sputtered amorphous tungsten oxide films, Solid State Ionics 165 (2003) 51– 58.

[10] D. L. Sun, S. Heusing, J. Puetz, M. A. Aegerter, Influence of water on the electrochemical properties of (CeO2)x(TiO2)1_x and WO3 sol–gel coatings and electrochromic devices, Solid State Ionics 165 (2003) 181– 189.

[11] Carl M. Lampert, Smart Materials Chromogenic, Material Today (ISSN:1369 7021 © Elsevier Ltd 2004), March 2004 28-35.

[12] J. N. Yao, P. Chen, A. Fujishima, J. Electroanal. Chem. 406 (1996) 223.

[13] K. Bange, T. Gambke, Adv. Mater. 2 (1990) 10.

[14] Vondrák J., Sedlaríková M., Hodal T.: Polymer Gel Electrolytes for Electrochromic Devices, Electrochimica Acta 44 (1999) 3067

[15] J. N. Yao, K. Kashimoto, A. Fujishima, Nature 355 (1992) 624.

[16] M. R. Tubbs, Phys. Status Solidi A 21 (1974) 253.

[17] C. Bechinger, S. Ferrere, A. Zaban, J. Sprague, B. A.Gregg, Nature 383 (1996) 608.

[18] R. D. Rauh, Electrochim. Acta 44 (1999) 3165.

[19] R. J. Mortimer, Electrochim. Acta 44 (1999) 2971.

[20] K. Bange, Sol. Energy. Mater.Sol. Cells 58 (1999) 11.

[21] H. H Wang, M. M. Yan and Z.Y Jiang, Electrochromic properties of rhodium oxide films prpepared by sol-gel method, Thin Solid Films 401 (2001) 211-215.

[22] A. Azens, G. Vaivars, M. Veszelei, L. Kullman and C. G. Granqvist, Eelctrochromic Design With Chemical Compatibility: Devices With W Oxide / Ni Oxide Tandem Layers, Proceeding of 4th International Meeting on Electrochromism (IME-4), Uppsala, Sweden, 21-23, Aug., 2000.

[23] P.van der Sluis, V. M. M. Mercier, Electrochimica Acta, 46 (2001) 2167-2171.

[24] Nagai J., Mc Meeking G. D., Saitoh Y., Solar Energy Materials and Solar Cells 56 (1999) 309-319.

[25] A. Bessiere, J. C. Badot, M. C. Certiat, J. Livage, V. Lucas, N. Baffier, Electrochimica Acta, 46 (2001) 2251-2256.

[26] G. Vaivars, A. Azens and C. G. Granqvist, Proton Conducting Polymer Composites for Electrochromic Devices, Proceeding of 4th International Meeting on Electrochromism (IME-4), Uppsala, Sweden, 21-23, Aug., 2000.

[27] M. Schmitt, M. A. Aegerter, Electrochimica Acta, 46 (2001) 2105-2111.

[28] T. V. Magdesieva, I. V. Zhukov, L. G. Tomilova, O. V. Korenchenko, I. P. Kalashnikova, and K. P. Butin, Electrochemical and electrochromic properties of rare-earth metal diphthalocyanine complexes, Physical Chemistry, 3 (2001) 396.

[29] N. Yashiwazaki, J. Appl. Phys. 31(6A) (1992)1892.

[30] Lin-Chi Chen, Kuo-Chuan Ho, Electrochimica Acta, 46 (2001) 2151-2158.

[31] Project Title: "NANOEFFECTS- Nanocomposites with High Colouration Efficiency for Electrochromic Smart Plastic Devices (Projecto Europeu de Investigação – 6FP-STREP-NMP3-CT-2003-505664), financiado pelo FP6- 6º Programa Quadro da Comunidade Europeia inserido na FP6 Thematic priority 3: Nanotechnologies and nanosciences, knowledge-based multifunctional materials and new production processes and devices (NMP).

[32] F. Michalak, P. Aldebert, Solid State Ionics, 85 (1996) 265.

[33] Project Title "Self Powered Integrated Photoelectrochromic Smart Window". Fundação para a Ciência e a Tecnologia (Portugal), http://www.fct.mces.pt/projectos/pub/2002/eng/index.asp ?dados=true&ficha=true&pID=48853&areaID=20.

Chapter 2 Experiments

2.1. Sputtering Technique

2.1.1. Introduction of sputtering

If ions or atoms with energy of several kilo-electron volts bombard a solid surface, atoms, molecules or clusters will be produced. Then they can be deposited on the surrounding wall of a vacuum chamber. This process, which is called sputtering, can be used to prepare thin films [1-2]. Sputtering has many advantages in film deposition. (i) Excellent film uniformity, particularly over large area; (ii) Surface smoothness and thickness control; (iii) The films have strong adhesion and are stable; (iv) Versatility: the sputter process is essentially a kinetic process involving momentum exchange rather than a chemical and thermal process and, therefore, virtually any material can be introduced into a gas discharge or sputtered from the solid; (v) High deposition rate, which is comparable to evaporation.

Normally sputtering processes are divided into four main categories: (i) dc (Direct current); (ii) rf (Radio frequency); (iii) magnetron; (iv) reactive. We recognize that there are important variants within each sputtering category (e. g., dc bias technique) and even hybrids between sputtering categories (e. g., reactive rf). However the commonly used sputtering techniques are dc magnetron and rf sputtering. In all cases the particles are ejected by the same basic mechanism of momentum exchange between energy particles and surface atoms.

2.1.2. Discharge of dc and rf sputtering

A schematic of a simplified sputtering system is shown in Fig. 2-1. The target is a plate of the materials to be deposited. It is connected to the negative terminal of a dc or rf power supply, so the target is also called cathode. After evacuation of the chamber the gas is introduced in which a discharge is initiated and sustained under the supply of power.

dc discharge. It is simplest case and gas discharge happen by applying a dc voltage between both electrodes. The dc sputtering is also known as diode of cathode sputtering.

rf discharges. Considerable charges arise in the discharge if high frequency electric field of more than 50 kHz is applied. The method of high frequency cathode sputtering differs from direct voltage in two main ways:

(a) The electrons that oscillate in the range of negative glow can gain sufficient energy to carry out more ionising collisions. This results in the discharge being less dependent on the emission of secondary electrons, and the "breakdown" voltage is reduced.

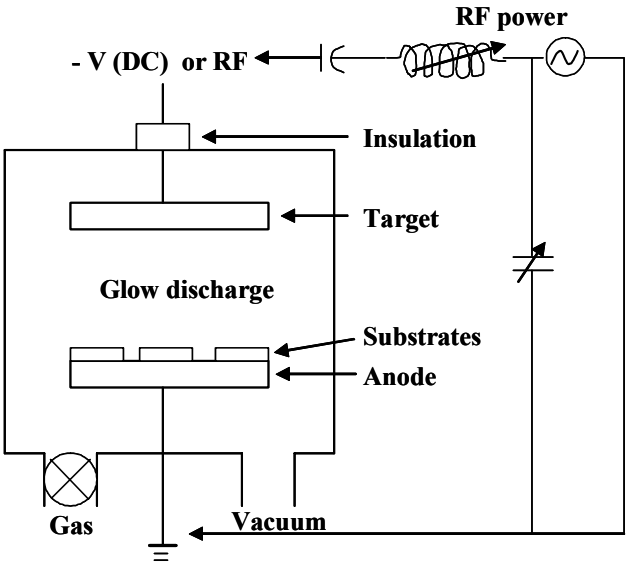

Fig. 2-1. Schematic of simplified sputtering system of dc and rf.

(b) The electrodes (target) need no longer to be electrically conductive since the rf voltage can be capacitive coupling. In principle, any material including insulators can therefore be used as rf target.

2.1.3. Magnetron target and bias sputtering

Magnetron sputter target. The class of sputter targets called magnetron has a magnetic field from 50 to 500 gauss parallel to the target surface. The magnetron field combining with the electric field causes the secondary electrons to drift in a closed circuit or magnetron tunnel in front of the target surface [2]. This electron confinement significantly increases the efficiency, and as a result, a magnetron make the sputtering operate at low gas pressures and low electric voltage.

Bias. Bias sputtering has been effective in altering a broad range of properties in deposited films. It is done by applying a bias potential (U_{bias}) during deposition of the film. If U_{bias} is negative the surface is bombarded by positive ions. If U_{bias} is positive electron and negative ions bombard the surface. The electron bombardment gives energy

to the already deposited material, so they can diffuse until occupying crystal positions. The films deposited with electron bombardment are of more crystalline (Section 7.3.3).

2.1.4. Reactive sputtering

Reactive sputtering is a method to deposit films which have a different composition than that of the target by adding gases into the sputtering chamber. A reaction of the gas with target material happens during deposition. Reactive sputtering has shown itself to be a very versatile technique capable of straight forward synthesis of broad materials [4-6]. Reactive sputtering allows precise control over coating structure and composition, and its coating performances are better than those achieved with conventional evaporation techniques in some cases.

In reactive sputtering the target is usually pure metal, alloy, or mixture of species which one desires to synthesise into a compound by sputtering in reactive gas or an inert gas-reactive gas mixture. The reactive gas is either, or contains the ingredient required to synthesise the desired compound. Another type of reactive sputtering involves a compound target that chemically decomposes substantially during inert gas ion bombardment, resulting in a film deficient in one or more constituents of the target. In this case, reactive gas is added to make up for the lost constituent. The main difference between these two types of reactive sputtering has to do with the deposition rate dependence on the partial pressure of the reactive gas. In our experiments the deposition of WO_3, V_2O_5, ZrO_2 and SnO_2 films belong to former type, the deposition of ITO film is later type.

At a very low reactive gas partial pressure and high target sputtering rate, it is well established that virtually all of the compounds synthesis occurs on the substrate surface. The stoichiometry of the film depends on the relative rates of the metal vapor and the reactive gas which arrives at the substrate. Under those conditions, the rate of removal and/or decomposition of compounds at target surface are far faster than the rate of compound formation at the target surface. However, as the reaction partial pressure is increased/or the target sputtering rate is decreased, a threshold is reached at which the rate of target compound formation exceeds the removal rate of the compounds. For a metal target, this threshold is usually accompanied by a sharp decrease in the sputtering rate. This decrease is due partially to the fact that oxides have generally lower sputtering rates than metals and that compounds have higher secondary electron emission yields than metals. As a result, more of the energy of incoming ions is used to produce and accelerate secondary electrons. With constant power supplies, the increased secondary

electron current automatically decreases the target voltage for a fixed power setting. Another cause of drop in the sputtering rate is simply due to less efficient sputtering by reactive gas ions than by inert gas ions.

2.1.5. Homemade dc-magnetron reactive sputtering system

A homemade dc-magnetron reactive sputtering system was used to deposit the films. The configuration and a photograph of the sputtering system are shown in Fig. 2-2 and Fig. 2-3. The substrate that faces the cathode may be grounded, heated, electrically floating, biased positively (or negatively), or some combination of these. The characteristics of the setup have been reported elsewhere [7].

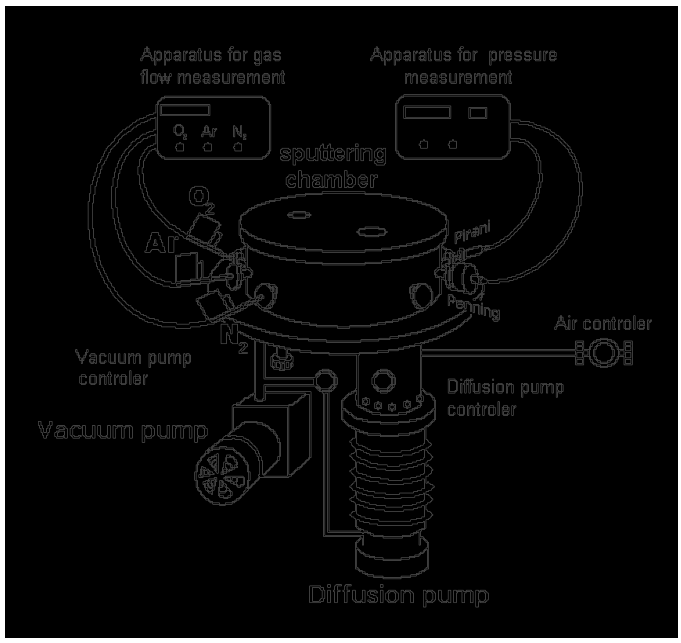

Fig. 2-2. Scheme of dc sputtering system.

The base pressure of the vacuum chamber was pumped to less than 1×10^{-3} Pa by mechanical and oil diffusion pumps before deposition. The pressure of the chamber is measured by a Pirani Gauge for the rough vacuum and a Penning for the secondary vacuum. The sputtering gas (Ar) and reactive gas (O_2) were introduced into the chamber separately, and were controlled through two gas mass flow rate controllers. The ratio of oxygen partial pressure is defined as P_{O2}= P (O_2)/[P (O_2)+ P (Ar)], where P (O_2) and P (Ar) are the gas pressures (by penning). The P_{O2} was varied in the experiments. To control the structure and stoichiometry of the films, different Ar and O_2 mixtures were used as sputtering gases. Argon (99.999% purity) or argon/oxygen (99.99%) mixtures were used as the pre-sputtering gas or sputtering gas.

Fig. 2-3. Photograph of dc sputtering system.

2.2. Preparation of the Films

The metal oxide films prepared in this work were all deposited by dc reactive magnetron sputtering. The commercially available high purity targets that were used were from Goodfellow Cambridge Limited. Sputtering was done with different $Ar+O_2$ mixture atmospheres. If the deposition process took place at room temperature (RT), a post-deposition annealing was possibly then performed from 80 to 600 ^{0}C (15-60 minutes).

To study the influence of the sputtering parameters on the structure and the properties of films, the films were deposited with different sputtering conditions, such as P_{O2}, total sputtering pressure (P_T), substrate temperature (T_S), sputtering power, and substrate-target distance, keeping the others constant. Transition metal oxide films doped with different Fe and Mo concentrations were also prepared. The detail deposition conditions for the films are listed in the tables of relevant chapter 4- chapter 8 (or Appendix I- List of the tables of sample names for electrochromic devices) and following parts.

2.2.1. ITO film deposition

The ITO target that was used had a diameter 85 mm, and contained pure In_2O_3 and 1 0 wt % SnO_2-doped. Sputtering was done at 1.0×10^{-1} and 1.2 Pa total work pressure. The purity of ITO targets commercially available is high 99.9% purity. The applied sputtering power was 40-78 W.

2.2.2. WO_3 film deposition

The tungsten target was composed of a compressed tungsten powder with 99.95% purity. The applied sputtering power was 85-102 W. Sputtering was done at a 1.3 Pa total work pressure. The optimisation of the WO_3 films was done by applying a bias potential (U_{bias}) during deposition. Films of tungsten oxides mixed with another transition metal oxide (molybdenum oxide) were deposited too.

2.2.3. V_2O_5 film deposition

The diameter of the vanadium target with a purity of 99.5% was 85 mm. The sputtering power applied was 95-100 W. Sputtering was kept at 6×10^{-1} Pa and 1.2 Pa total work pressure. Films of vanadium oxides (V_2O_5) mixed with another transition metal molybdenum oxide were deposited too.

2.2.4. ZrO_2 film deposition

The area of the zirconium target with a purity of 99.8% was 100 × 100 mm. The applied sputtering power was 80-90W. Sputtering was done at 5×10^{-1} Pa total work pressure.

2.2.5. SnO_2 film deposition

The Sn target was composed of a compressed tin powder with 99.95% purity. The applied sputtering power was 100-125 W. Sputtering was done from 5×10^{-1} Pa to 3.0 Pa total work pressure. The optimisation of the SnO_2 films was done by applying a bias potential (U_{bias}) during deposition. 99.5% purity iron (Fe) was added to get doped tin oxide films.

2.2.6. CdS film deposition

The CdS films with ultrafine particles (UFP) were obtained by a so called “ultrasonic colloid deposition (USCD)” method. Our experimental setup is shown schematically in Fig. 2-4. It consists of two main parts. The first is the reaction bath, in which the

temperature of the bath is monitored to maintain a constant temperature. The second is the ultrasonic part whereby the frequency and intensity of the ultrasonic can be controlled and maintained at a constant level. The CdS films were deposited on normal microscope slides, ITO and quartz substrates. The deposition solution was prepared by mixing up 200mL of 0.01 mol/L $CdCl_2$, 0.038 mol/L NH_4Cl and 0.78 mol/L NH_4OH with 200mL of 0.16 mol/L Thiourea [$S=C(NH_2)_2$], 0.038 mol/L NH_4Cl and 0.78 mol/L NH_4OH in a beaker. The beaker was placed in a water bath with an ultrasonic generator. The cleaned substrate was then immersed in the deposition bath, and the temperature of the solution was adjusted in the range 60-90 ^{0}C. The chosen frequency was 42 kHz. The power of ultrasonic was more than 50 Watts. The pH value of the combined solution was 11.8.

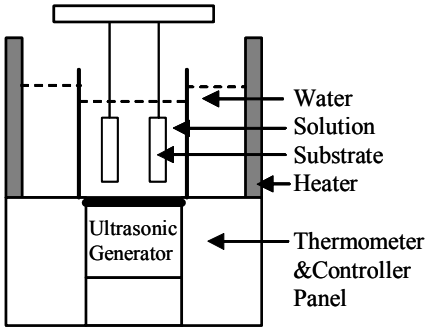

Fig. 2-4. Experimental setup of the ultrasonic colloid deposition (USCD) method.

2.2.7. Annealing of the film samples

Annealing was done in air with a Termolab Oven (Fornos Eléctricos LDA, 0-1999 ^{0}C temperature range) and in vacuum with the sputtering chamber (Home-made, 2.5 Pa pressure, 0-400 ^{0}C).

2.3. Measurements of the Film Samples

2.3.1. Measurements of transmittance, absorptance, diffuse and specular reflectance

The film transmittance, absorptance, diffuse and specular reflectance spectra were measured in UV-visible-near infrared region by a double beam Shimadzu UV-3101PC spectrophotometer, which is available for wavelengths in the range 200 nm – 3200 nm.

For optical constant calculation of the films, the transmittance spectra were measured in the region 300 nm - 3200 nm. The samples measured in transmission were irradiated under perpendicular incidence angle. The specular reflection measurements were carried out under an incidence angle of 8^0. The diffuse and specular reflectance spectra of the films were measured by using an integrating sphere attachment which can be mounted in the sample compartment of the spectrophotometer. The integrating sphere has an internal diameter of 60 mm. The detectors are photomultiplier and PbS cell.

In the measurements of the diffuse reflectance spectra, two standard white plates were put on the sample side and the reference side for making the baseline correction. Then, the standard white plate was exchanged with a film sample facing the light source for the measurement. The specular reflectance spectra were measured with the same system as used for measuring the diffuse reflection spectra of the films, but the standard mirror was put on the sample side for baseline correction. After making the baseline, the standard mirror was exchanged with a film sample for measurement.

2.3.2. Measurement of IR spectra of the films

The ex-situ IR spectra of the films were obtained using a Fourier-transform infrared (FT-IR) Bio-Rad FTS135 spectrometer (spectral range 4000-400 cm^{-1}). Reflective absorption spectra in the mid-infrared were investigated in the films. The IR technique of reflective absorption is chose in case of near graze incidence angle (NGIA). The background spectra were scanned with an Al (aluminium) mirror as the reference. The resolution in wavenumber is 2 cm^{-1}.

2.3.3. Measurement of Raman spectra of the films

The Raman spectra of the films were measured using a JOBIN-YVON T64000 triple Raman spectrometer with a Cohereent Innova 92 Ar ion laser. The T64000 system is a fully computerized, triple spectrograph system, and has micro and macro sample chambers. The T64000 system offers a charge-coupled-device (CCD) multichannel detector and a photomultiplier tube (PMT) monochannel detector for selection. The CCD detector was used in our work. The resolution is better than 2 pixels and the wavenumber accuracy is ± 1 cm^{-1} when using the CCD detector.

The Raman spectra of the films were measured using a microanalysis system. The laser light with the wavelength of 514.5 nm was focused on the films through an Olympus BH2- UMA microscope. The focused beam spot size is about 1 μm with the

objective magnification of 100. The laser power was measured by a Coherent Labmaster-E laser power meter with the laser beam focusing on the sensor through the objective of the microscope. To prevent the influence of the temperature in the Raman during the measurement, the temperature of the laboratory was controlled at 21^{o}C for all the measurements.

2.3.4. AFM, SEM and EDX measurements

The film surface morphology and cross section structure were observed by SEM (scanning electronic microscope, UK Leica-Cambrigde S360, Japan Hitachi model S-2400, Japan JEOL-JXA-840) and AFM (atomic force microscopy, Multimode TM SPM 3, Digital Instruments Nanoscope). In order to prevent charge build-up, a thin gold film was sputtered on the surface and cross section of the samples before measurement on the SEM. EDX (Energy Dispersive X- ray) was employed to analyze the stoichiometry of the film and the doped material concentration. The used EDX is a Link eXLII –pentafet Oxford (UK) combined with SEM system- S360.

2.3.5. X-ray diffraction (XRD) and GIXD

Data of XRD (x-ray diffraction) and GIXD (grazing incidence X-ray diffraction) were taken in a computer-controlled Philips PW-1710 diffractometer and a Simens D5000 with KRISTALLOFLEX 710 X-ray generator. Cu Kα radiation ($K\alpha_1$: 1.54056 Å, $K\alpha_2$: 1.54439 Å, 40 kV, 20mA) from an X-ray tube with normal focus was used. The basic principle of X-ray diffraction is described elsewhere [8].

2.3.6. X-ray photoelectron spectroscopy

The atomic composition and the chemical state of the films were studied by X-ray photoelectron spectroscopy (XPS) [9] using an ESCALAB MK2 (VG Inc. UK). MgKα line at 1253.6 eV was used in the measurements. The analysis chamber was at 10^{-7} Pa or better. Binding energies were referenced to the C1s level of the carbon at 284.6 eV. Region characteristic for signal was run in high-resolution mode using 0.2 eV step.

2.3.7. Measurements of the thickness, roughness, electrical and optical properties of the films

The sheet resistance (R_s) was determined using a home made four-point-probe system (described in Chapter 3). The film resistivity was measured by a Veeco FPP-5000 four-point probe. Van der Pauw and Hall Effect measurements were used in order to

determine carrier concentration (n_c) and carrier (or Hall) mobility (μ). The magnetic intensity is about 0.4 T.

The ellipsometric parameters Psi and Delta were measured by using a Jobin-Yvon UVISEL variable angle ellipsometer at 55^0 incidence angle over the spectral range 400–800 nm with 1 nm step. From Psi and Delta data the refractive index *n* and extinction coefficient *k* as a function of the wavelength was obtained for ITO films prepared at different conditions. Film thicknesses were obtained by a transmittance interference spectrum method (Section 3.6) and an ellipsometric method. They were confirmed by SEM results. Film roughness was measured and obtained by a TIS (total integrated scattering) spectrum method (Section 3.3) and AFM observation. The thickness and roughness were also valued by LIMT (laser triangulation based micro-topographer) method (Section 9.4.5).

2.4. References

[1] Donald H. Mattox, Handbook of Physical Vapour Deposition (PVD) processing: Film Formation, Adhesion, Surface Preparation and Contamination Control Noyes Publication, ISBN 0-8155-1422-0 (1998)

[2] N. Schwartz, P. W. Perry, Physics of Thin Films(G.Hass, R.E.Thun eds.), Vol.2, p.363, Academic Press, New York, 1964.

[3] J. A. Thornton, A.S.Panfold, "Thin Films Processes" (J.L. Vossen, W.Kern, eds.), p.75, Academic Press, New York, 1978.

[4] W. T. Pawlewicz, R. Busch, Thin Solid Films, 63 (1979) 251.

[5] T. Nyerg, C. Nender, S. Berg, J. Vac. Sci. Technol., 6 (1998) 1868.

[6] C. Park, Y. Ma, H. Kim, J. Appl. Phys. 81 (1997) 7764.

[7] J. B. Almeida, Vacuum, 39 (1989) 717.

[8] B. D. Cullity, Elements of X-ray Diffraction (2nd edition), Addison-wesley publishing company, Inc. (Reading-UK, Massachusetts, USA) 1978.

[9] Čechal J., Tichopadek P., Nebojsa A., Bonaventurova O., Urbanek M., Spousta J., Navratil K., Šikola, T., In situ analysis of PMPSi by spectroscopic ellipsometry and XPS, Surface and Interface Analysis, vol. 38(2004)8

Chapter 3 Theories and Methods on Characterization of the Films

This chapter contains some theories and methods of the experiments for characterizing of the films. We give only explanations on the theories and methods which are treated or selected for use in the experiments. General theories and methods for applications it can be found in relevant field references.

3.1. Reflection Spectroscopy of Thin Films

3.1.1. Introduction of reflection spectroscopy of films

Transmission or absorption measurements have been normal practice for samples in spectroscopy. However reflection has some advantage for thin film sample. In the section 3.1 we summarize the reflection spectrum techniques for film sample analysis.

Generally reflection spectrum techniques include. (a) ATR (attenuated total reflection) or internal reflection. (b) Specular reflection. (c) Diffuse reflection. (d) Reflection-absorption. (b)~(d) are also called external reflection [1-2] .

Advantage of Reflection spectroscopy: It does not need sample preparation. ATR and Reflection-absorption can also be used to study the orientation of the molecules in the film by using a polarizer.

Disadvantage of Reflection spectroscopy: low intensity of signal.

3.1.2. Attenuated total reflection (ATR)

In Fig. 3-1 part a, if n_1 is the refractive index of the film or sample, n_2 is that of the internal reflection element (IRE) material in the ATR system and α is an incidence angle (between incidence light and vertical line of interface of ATR or sample), then the total internal reflection occurs if $\alpha >$ or $= \alpha_c$, where the critical angle α_c is given by:

$$\sin\alpha_c = n_1 \bullet \sin 90^0 / n_2 = n_1 / n_2.$$

3.1.3. Specular reflection

For specular reflection studies the samples have a smooth surface. The incident radiation partly penetrates into the sample and is partly reflected. Generally, normal transmission and specular reflection spectra have little resemblance, and only strong absorption bands can be studied. Thus specular reflectance spectroscopy is not a very

workable technique. However, it is useful for measurements of optical constants. In this work we mainly used it as a tool to determine the surface constants of the films.

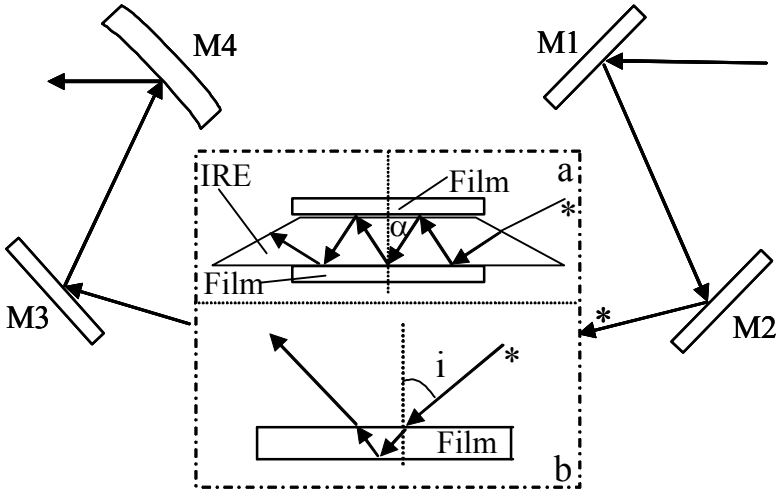

Fig. 3-1. IR reflectional optic diagram, a.) ATR attachment with trapezoid internal reflection element (IRE), b.) external reflection case.

3.1.4. Diffuse reflection

The diffuse reflection has been widely used for UV-Vis-NIR ranges, but it was hardly used in mid-IR region. With increasing surface roughness, specular reflection decrease, whereas there is a growing diffuse reflection. Normally the technique is suitable for powder specimen. The incident radiation penetrates the top layer of the powder and into the inside of sample. Then it returns in any direction after a complicated process of scattering and refraction in the bulk of the sample. Here we will investigate the characterization and properties of the films using the diffuse reflection technique in UV-Vis-NIR region.

3.1.5. Reflection-absorption and near grazing incidence angle (NGIA)

Reflection-absorption is a special case of reflection spectroscopy at fixed incidence angle (part b in Fig. 3-1). It is found that the intensity of the spectrum becomes stronger with increasing incidence angle (θ_i: between incidence and vertical line of the surface of film). At near grazing incidence angle (θ_i =~88 ^{0}), the absorption intensity reaches a maximum. The incident radiation penetrates into the thin film and is reflected on the interface of sample and substrate, thus passing the layer twice. The sample usually is a thin layer of material supported by a smooth surface (substrate or a metal surface).

3.2. Reflective IR Spectra of the Film on Glass Substrates

3.2.1. Infrared (IR) spectra

Since early Infrared (IR) spectrometers had restricted range and low sensitivity, they limited the applications in inorganic compounds, especially in the film field. After technical advance of IR, it became clear that Fourier Transform IR (FTIR) could provide a wealth of information from bulk inorganic compounds and thin films. Some information is unique only to the IR technique.

IR structural studies of WO_3, $WO_3 \bullet xH_2O$ and other material films are particularly necessary. Since the films adsorb molecular water at their external surfaces during preparation and storage, it is very helpful to be able to distinguish adsorbed molecular water from structure and surface. Due to the IR high sensitivity to the presence of OH (hydroxyl) group, direct experimental proof of the presence of water in the films can be deduced from the IR spectrum.

3.2.2. Problem of IR measurement in EC windows

Generally there is a problem in IR measurements of the film that is deposited on a glass substrate. It can not directly measure the film on glass substrate, because the glass has limited infrared transmittance in the range 2000-4000 cm^{-1} for normal IR spectrometers. Since inorganic materials have structure information in the IR range 400-2000 cm^{-1}, and WO_3 or V_2O_5 films should be deposited on normal glass for the smart window application, we have to use a IR method for analysis of these films, thus, the reflective absorption spectrum measurement was proposed for investigating WO_3 and V_2O_5 films in the mid-infrared (Section 3.1.5).

3.3. Surface Roughness (δ) and Total Integrated Scattering (TIS) of the Films

In most cases surface roughness (δ) is an important data of the thin film. The δ parameter corresponds to the standard deviation of the micro-geometric surface height (or peaks and valleys). It can be obtained from the total integrated scattering (TIS). The TIS is defined as the ratio of the light scattered by diffuse reflectance to the total reflectance (specular plus diffuse reflectance) of the surface [3-4].

$$TIS=\frac{\text{diffuse reflectance}}{\text{specular reflectance}+\text{diffuse reflectance}}=1\text{-}\exp\text{-}\left(\frac{4\pi\delta\cos\theta_0}{\lambda}\right)^2 \qquad (3.1)$$

where θ_0 is the angle of incidence. If the surface roughness δ is much smaller than the wavelength λ, then

$$\text{TIS} \approx \left(\frac{4\pi\delta\cos\theta_0}{\lambda}\right)^2 \qquad \text{Thus} \quad \delta = \frac{\lambda}{4\pi\cos\theta_0}\,(\text{TIS})^{1/2} \tag{3.2}$$

We can calculate the δ value by Equation (3.2).

3.4. Vibration Spectra

The vibration spectrum results from the absorption of electromagnetic radiation in the infrared region which results in changes in the vibration energy of the molecules. Though some spectroscopies such as inelastic neutron scattering see changes in the vibration energy of a molecule, generally vibration spectrum means infrared (IR) and Raman spectroscopy.

Since, usually all molecules have vibrations in the form of stretching, bending, etc., the absorbed energy will be utilised in changing the energy levels associated with these. This is a valuable tool in identifying compounds. To analyse compounds which are not responding to IR, Raman is an alternate to IR. Raman involves the scattering of mono-wavelength incident radiation on molecules in its vibration energy at a vertical direction of the incidence light.

IR and Raman spectroscopy have close relationship, they both allow the study of vibration and rotation of molecules, but they work in different mechanisms. Infrared spectroscopy studies the absorption spectrum after the incident radiation passes through the samples, whereas Raman spectroscopy studies the scattering radiation which is excited by the incident radiation. The Raman technique uses a visible or ultraviolet spectrometer. Raman and IR spectroscopy can be regarded as complementary, rather than alternative or duplicative methods of investigating transitions between energy levels of molecules.

Although IR and Raman spectroscopies are similar in providing information on vibration frequencies, there are many differences between them. Some vibrations are only Raman active while others are only IR active; the vibration of a heteropolar diatomic molecule is IR active, whereas that of a homopolar diatomic molecule is not

IR active. If a macromolecule has a local center of symmetry of chromophore or more, its vibration is IR active, Raman active, or active in both. However, totally symmetric vibrations are always Raman active.

3.5. Raman Spectra

When monochromatic radiation of wavenumber $\tilde{\nu}_o$ is incident on a system some scattering of the radiation occurs. If the frequency content of the scattered radiation is analysed, it will present not only the wavenumber $\tilde{\nu}_o$ associated with the incident radiation but also, pairs of new wavenumbers of the type $\tilde{\nu}' = \tilde{\nu}_o \pm \tilde{\nu}_M$. In molecular systems, the wavenumbers $\tilde{\nu}_M$ are found to lie principally in the ranges associated with transitions between rotational and vibration levels. The scattered radiation usually has polarisation characteristics different from those of the incident radiation, and both the intensity and the polarisation of the scattered radiation depend on the direction of observation. Such scattering of radiation with change of frequency (or wavenumber) is called Raman scattering. The scattering of radiation without change of frequency is called Rayleigh scattering [5-6]. Such scattering arises from scattering centers, like molecules, which are very much smaller than the wavelength of the incident radiation. Raleigh scattering always accompanies Raman scattering and can be observed with Raman scattering.

In the spectrum of scattered radiation, the new wavenumbers are named Raman lines, or bands, and collectively are said to constitute a Raman spectrum. Raman bands at wavenumbers less than the incident wavenumber (i.e., of the type $\tilde{\nu}_o$ - $\tilde{\nu}_M$) are referred as Stokes bands, and those at wavenumbers greater than the incident wavenumber (i.e., $\tilde{\nu}_o$ + $\tilde{\nu}_M$) as anti-Stokes bands.

The origin of the modified frequencies found in Raman scattering may be explained in terms of energy transfer between the molecule scattering system and the incident radiation. When a system interacts with radiation of wavenumber $\tilde{\nu}_o$, it may make upward transition from a lower energy level E_1 to a higher energy level E_2. It must then acquire the necessary energy, $\Delta E = E_2 - E_1$, from the incident radiation. The energy ΔE may be expressed in terms of a wavenumber $\tilde{\nu}_M$ associated with the two levels involved, where $\Delta E = hc\,\tilde{\nu}_M$. This energy requirements may be regarded as being

provided by the annihilation of one photon of the incident radiation of energy $hc\tilde{\nu}_o$ and the simultaneous creation of a photon of smaller energy $hc(\tilde{\nu}_o - \tilde{\nu}_M)$, so that scattering of radiation of lower wavenumber, $\tilde{\nu}_o - \tilde{\nu}_M$, occurs. Alternatively, the interaction of the radiation with the system may cause a downward transition from higher energy level E_2, if the system happens already to be in that excited level, to a lower energy level E_1, in which case it makes available scattering of radiation of higher wavenumber, $\tilde{\nu}_o + \tilde{\nu}_M$.

In the case of Rayleigh scattering, although there is no result change in the energy state of the system, it still participates directly in the scattering process, causing one photon of incident radiation $hc\tilde{\nu}_o$ to be annihilated and a photon of the same energy to be created simultaneously, so that scattering of radiation of unchanged wavenumber, $\tilde{\nu}_o$, occurs.

It is clear that, as far as the wavenumber is concerned, a Raman band can be characterized not only by its absolute wavenumber, $\tilde{\nu}' = \tilde{\nu}_o \pm \tilde{\nu}_M$, but also by the magnitude of its wavenumber shift $|\Delta\tilde{\nu}|$ from the incident wavenumber, where $|\Delta\tilde{\nu}| = |\tilde{\nu}_o - \tilde{\nu}| = \tilde{\nu}_M$. Such wavenumber shifts are often referred as Raman wavenumber or Raman shifts. Where is necessary to distinguish Stocks and anti-Stokes scattering we shall define $\Delta\tilde{\nu}$ to be positive for Stokes scattering and negative for anti-Stokes scattering, that is $\Delta\tilde{\nu} = (\tilde{\nu}_o - \tilde{\nu}')$. Unless small values of wavenumber shifts are involved, it is Stokes Raman scattering which is mainly studied, since the intensity of anti-Stokes Raman scattering decreases rapidly with increasing wavenumber shift. This is because anti-Stokes Raman scattering involves transitions to a lower energy state from a populated higher energy state. The thermal population of such higher states decreases exponentially as their energy, $hc\tilde{\nu}_M$, increases above the lower state.

Stokes Raman scattering is related to the molecule at an excited state and anti-Stokes scattering is related with the molecule at the ground state. The intensity of Stokes and anti-Stokes Raman bands is proportional to the number of correspondent energy states. Generally, the distribution of the molecules with the vibration energy is given,

$$dN \propto e^{-E/KT} dE \qquad (3.3)$$

where dN is the molecule number distributed in a vibration energy range of dE. $e^{-E/KT}$ is the Boltzmann factor. It can be found that the distribution of the molecules decreases

rapidly with the increase of vibration energy from Equ. (3.3). Therefore the anti-Stokes Raman scattering is weaker than that of Stokes Raman scattering.

We have discussed Raman theory for molecule systems. For the crystalline materials, it can be regarded as a mechanical system of nN particles, where n is the number of particles (atoms) per unit cell and N is the number of primitive cells contained in the crystal. Since N is very large, a crystal has a huge number of vibrations. However, the observed spectrum is relatively simple because only where equivalent atoms in primitive unit cells are moving in phase they are observed in the Raman spectrum. Considering the vibration frequencies in a crystal, the vibrations can be divided into an optical branch or optical phonon (relates to the Raman scattering, the frequencies occurring in the optical spectral region) and an acoustic branch or acoustic phonon (the frequencies occurring in the sonic or ultrasonic region). The local symmetry of a crystal in a particular phase is manifested in the appearance of discrete vibrational modes which serve to identify that phase. In the isomorphic amorphous materials, vibrational bands broaden and intensities decrease, resulting in a spectrum that is the envelope of sharp lattice features associated with the crystalline phase. Nevertheless, molecularly specific information can be obtained from Raman spectra of both amorphous and crystalline materials.

3.6. Refractive Index (n), Extinction Coefficient (k), Thickness (d) and Interference Transmittance Spectra

Refractive index (n), extinction coefficient (k) and thickness (d) are important parameters for predicting the performance of a film in an optical system. These optical parameters are also sensitive to the microstructure, which is affected by the deposition conditions and doping materials, as well as by the dopant concentration.

Several methods have been used to determine the optical constants of thin films based on the measurement of intensity of the reflected, absorbed and/or transmitted light as a function of wavelength and/or angle of incidence [7-9]. Among these methods, the one given by Swanepoel is widely used because of its simplicity [10-12].

Consider that a film has thickness d and complex refractive index $\tilde{n} = n - ik$, where n is the refractive index and k is the extinction coefficient which can be expressed in terms of the absorption coefficient α. The transparent substrate has a thickness several

orders of magnitude larger than the film, and has refractive index s and absorption coefficient $\alpha_s = 0$. The refractive index of the surrounding air is $n_o = 1$.

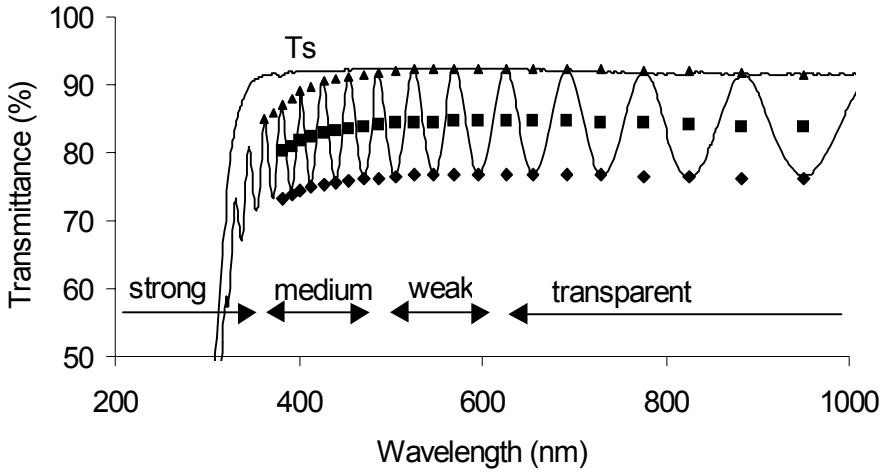

Fig. 3-2. The transmission spectrum of a film on a finite glass substrate. T_s (curve): substrate; T_M (▲): maximum envelope of interference; T_m (♦): minimum envelope of interference; and T_α (■): interference-free.

If the thickness d is not uniform or is slightly tapered, all interference effects are destroyed and the transmission is a smooth curve as shown by the square curve Tα in Fig. 3-2. The spectrum can be roughly divided into four regions. (a) Transparent region: in this region $\alpha = 0$ and the transmission is determined by n and s through multiple reflections. (b) Weak absorption region: in this region α is small but starts to reduce the transmission. (c) Medium absorption region: in this region α is large and the transmission decreases mainly due to effect of absorption. (d) Strong absorption region: in this region the transmission decreases drastically due almost exclusively to the influence of α.

If the thickness d is uniform, interference effects give rise to a spectrum shown by the full curve in Fig. 3-2. These fringes can be used to calculate the optical constants of the thin film as shown below.

As we know, the basic equation for interference fringes is

$$2nd = m\lambda \tag{3.4}$$

where m is an integer for maxima and half integer for minima.

The rigorous expression for the transmission (T_l) for the system as shown in Fig. 3-2 is [10],

$$T_l = \frac{A'x}{B' - C'x + D'x^2} \tag{3.5}$$

where

$$A' = 16s(n^2 + k^2)$$

$$B' = \left[(n+1)^2 + k^2\right] \cdot \left[(n+1)(n+s^2) + k^2\right]$$

$$C' = [(n^2\text{-}1\text{+}k^2)(n^2\text{-}s^2\text{+}k^2)\text{-}2k^2(s^2\text{+}1)]2\cos\phi \text{ -}k[2(n^2\text{-}s^2\text{+}k^2)\text{+}(s^2\text{+}1)(n^2\text{-}1\text{+}k^2)]2\sin\phi$$

$$D' = \left[(n-1)^2 + k^2\right] \cdot \left[(n-1)(n-s^2) + k^2\right]$$

$$\phi = 4\pi nd/\lambda, \quad x = \exp(\alpha d), \quad \alpha = 4\pi k/\lambda$$

The expression (3.5) becomes much simpler if we put k = 0. This is an approximation that is valid over most of the region of the spectrum in Fig.3.2. In the situation the equation (3.5) becomes:

$$T_l = \frac{Ax}{B - Cx\cos\phi + Dx^2} \tag{3.6}$$

where

$$A = 16n^2 s \tag{3.6a}$$

$$B = (n+1)^3 (n+s^2) \tag{3.6b}$$

$$C = 2(n^2 - 1)(n^2 - s^2) \tag{3.6c}$$

$$D = (n-1)^3 (n-s^2) \tag{3.6d}$$

$$\phi = 4\pi nd/\lambda \tag{3.6e}$$

$$x = \exp(\alpha d) \tag{3.6f}$$

The extremes of the interference fringes can be written as,

$$T_M = \frac{Ax}{B - Cx + Dx^2} \tag{3.7}$$

$$T_m = \frac{Ax}{B + Cx + Dx^2} \tag{3.8}$$

For further analyses T_M and T_m are now considered to be continuous functions of λ. For any λ, T_M has a correspondent value T_m.

In the region of weak and medium absorption, $\alpha \neq 0$ and $x < 1$. Subtracting the reciprocal of Eq. (3.7) from the reciprocal of Eq. (3.8) yields an expression that is independent of x,

$$\frac{1}{T_m} - \frac{1}{T_M} = \frac{2C}{A} \tag{3.9}$$

Substituting Eq. (3.6) into (3.9) and solving for n yields,

$$n = \left[N + (N^2 - s^2)^{1/2}\right]^{1/2} \tag{3.10}$$

where

$$N = 2s\frac{T_M - T_m}{T_M T_m} + \frac{s^2 + 1}{2}$$

Eq. (3.10) can be used to calculate n(λ) from T_m and T_M. It is identical to the formula derived by Manifacier et al [8] using the theory for an infinite substrate.

Once n(λ) is known, all the constants in Eq. (3.6) are known and x can be calculated in various ways. Both Eq. (3.7) and (3.8) are quadratic equations in x that can be solved for x and the results simplified using Eq. (3.6). Solving Eq. (3.7) gives,

$$x = \frac{E_M - \left[E_M^2 - (n^2-1)^3(n^2 - s^4)\right]^{1/2}}{(n-1)^3(n - s^2)} \tag{3.11}$$

where

$$E_M = \frac{8n^2 s}{T_M} + (n^2 - 1)(n^2 - s^2)$$

Solving Eq. (3.8) gives,

$$x = \frac{E_m - \left[E_m^2 - (n^2-1)^3(n^2 - s^4)\right]^{1/2}}{(n-1)^3(n - s^2)} \tag{3.12}$$

where

$$E_m = \frac{8n^2 s}{T_m} + (n^2 - 1)(n^2 - s^2)$$

The interference-free transmission Tα can be calculated from the interference fringe by integrating Eq. (3.6) between a maximum and an adjacent minimum,

$$T_\alpha = \frac{1}{\pi}\int_o^\pi \frac{Ax}{B - Cx\cos\phi + Dx^2} d\phi \qquad (3.13)$$

Assuming a narrow intergrating region where all parameters are constant, the integral yields,

$$T_\alpha = \frac{Ax}{\left[(B - Cx + Dx^2)(B + Cx + Dx^2)\right]^{1/2}} \qquad (3.14)$$

Substituting equations (3.7) and (3.8) into (3.14) gives:

$$T_\alpha = (T_M \times T_m)^{1/2} \qquad (3.15)$$

Thus, T_α is just the geometric mean of T_M and T_m.

If n_1 and n_2 are the refractive indices at two adjacent maxima (or minima) at λ_1 and λ_2, it follows from Eq. (3.4) that the thickness is given by,

$$d = \frac{\lambda_1\lambda_2}{2(\lambda_1 n_2 - \lambda_2 n_1)} \qquad (3.16)$$

The x (λ) can be obtained from Eq. (3.11) or (3.12) and then α(λ) can be calculated by equation (3.6f). Once α(λ) is known, k(λ) can be determined from the equation:

$$k = \alpha\lambda / 4\pi \qquad (3.17)$$

which completes the calculation of the optical constants (Eq. (3.10) is used for the calculation of the refractive index n; Eq. (3.16) is used for the calculation of thickness; Eq. (3.6f), (3.11) and (3.17) is used for the calculation of extinction coefficient k).

3.7. Energy Band Gap (E_g)

In the strong and medium absorption region, the optical behavior of the films is dominated by the absorption from the valence electrons. The absorption coefficient α can be determined by [13-14]: $\alpha^N = C(h\nu - E_g)$, where N is dependent on the type of electron transitions, and E_g is the band gap. In case of direct and indirect transition semiconductor, N is 2 and 1/3 respectively. From the absorption data, it is then possible to obtain E_g for each film. There are different models and many reports about the absorption coefficient [15]. α is obtained from measurements of the absorption spectrum.

If α^2 is plotted vs. the photon energy (hν), extrapolating the linear region towards the hν axis gives the effective direct transition energy E_g.

3.8. AFM Analysis

The three dimensional (3D) morphology of films can be observed by AFM (atomic force microscopy). A quantitative method to examine the surface morphology and structure is obtained by analysing the surface roughness using AFM. It is based upon the ability to measure tiny forces acting upon a cantilever. The deflection of the cantilever is quantified by a laser reflection off the cantilever. The AFM images of the topography mapping are obtained by scanning the cantilever on the surface with a constant force. In taping mode a higher lateral resolution is achieved using lower forces. These do less damage to soft samples imaged in air, because the lateral forces are virtually eliminated [16-17].

The most important measurement of the surface roughness can be given with a statistical parameter-root mean square (rms or R_q) that is the standard deviation of the height (Z) values within a given area:

$$Rq = \sqrt{\frac{\sum_{i=1}^{N}(Z_i - Z_{ave})^2}{N}}, \qquad (3.18)$$

where Z_{ave} is the average of Z value within the given area, Z_i is the current Z value and N is the number of points within a given area.

The mean roughness (R_a) that represent the arithmetic average of the deviations from the median plane is also a widely used parameter.

$$Ra = \frac{\sum_{i=1}^{N}\left|Z_i - Z_{cp}\right|}{N}, \qquad (3.19)$$

where Z_{cp} is the Z value of the median plane, and Z_i is the current Z value and N is the number of points within a given area.

3.9. Measurement of Sheet Resistance of the Film

Sheet resistance (R_s) of the films is a common way to express values of thin film resistivity. Its unit is “ohms per square” or Ω/Sq. As we know, the Four-point probe method (Fig. 3-3a) was chosen to measure the R_s of the film. To explain it, let us

consider a model of a conductor film depicted in Fig.3-3 b. If the film length is L, width w, thickness d, and resistivity ρ, the film resistance is R= ρL/wd. In the special case of a square film with L=w, it becomes:

$$R=R_s= \rho/d \ (\Omega/Sq) \qquad (3.20)$$

which is called the sheet resistance of film. R_s is independent of the film dimensions other than thickness. Any square, irrespective of size, would have the same resistance. Electrostatic analysis of the electric potential and field distributions within the film yields

$$R_s= K(V/I) \qquad (3.21)$$

where K is a constant dependent on the configuration and spacing of the contacts. If the film is large in extent compared with the probe assembly and the probe spacing large compared with the film thickness, K= π/ln2=4.53 [18].

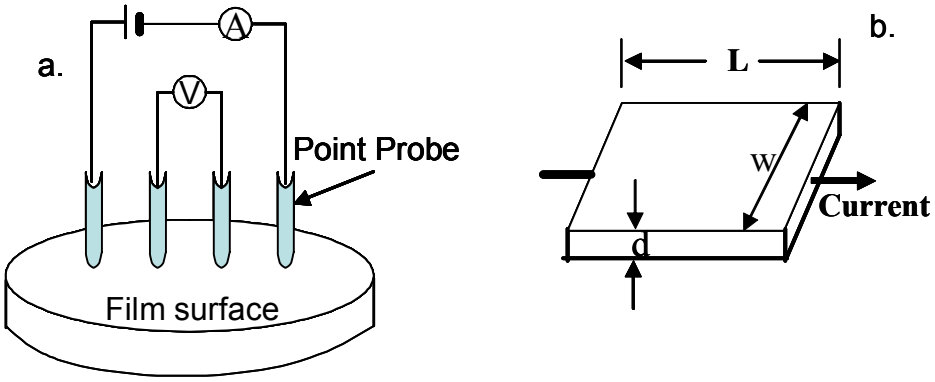

Fig. 3-3. (a) Four-point probe method for measuring the sheet resistance of thin film;

A: current meter and V: voltage meter; (b) a depicted model of the conductor film with length L, width w, and thickness d.

3.10. References

[1] Michael Bass, Handbook of Optiscs, McGraw-Hill, Inc. (USA), (1995) I-6.4, 6.5, II-35.2.

[2] H. A. Willis, J. H. van der Maas and R. G. J. Miller, Laboratory Methods in Vibrational Spectroscopy, 3rd Edition, John Wiley & Sons: New York (1987).

[3] K. H. Guenther, P. G. Wieder and J. M. Bennett, Appl. Op., 23 (1984) 3820

[4] H. E. Bennett and J. O. Porteus, J. Opt. Soc. Am., 51 (1961) 123.

[5] C. V. Raman, and K.S. Krishnan, Nature, 121 (1928) 501

[6] L. Rayleigh, Phil. Mag., XLI, 274 (1871) 447

[7] J. D. Klein, Y. Yen, and S. F. Cogan, J. Appl. Phys., 68 (1990) 1825

[8] J. C. Manifacier, J. Gasiot, and J. P. Fillard, J. Phys. E, 9 (1976) 1002

[9] R. Swanepoel, J. Phys. E, 16 (1983) 1214

[10] D. Wicaksana, A. Kobayashi, and A. Kinbara, J. Vac. Sci. Technol. A, 10 (1992) 1479.

[11] P. Gao, L. J. Meng, M. P. Dos Santos, V. Teixeira, M. Andritschky, Vacuum 56 (2000) 143.

[12] E. Marquez, J. Ramirez-Malo, P. Villares, R. Jimenez-Garay, P. J. S. Ewen, A. E. Owen, Calculation of the thickness and optical constants of amorphous arsinic sulphide films from their transmission spectra, J. Phys. D: Appl. Phys., 25 (1992) 535-541.

[13] C. H. L. Weihtens and P. A. C. Van Loon, Thin Solid Films, 196 (1991) 1.

[14] J.Szczyrbowski, A. Dietrichand H.Hoffmann, Phys. Status Solidi A, 78 (1983) 243

[15] M. Bender, W. Seelig, C. Daube, H. Frankenberger, B. Ocker, J. Stollenwerk, Thin Solid Films, 326 (1998) 72.

[16] Nanoscope III, dI Digital Instruments

[17] Serry F. M., Strausser Y. E., Elings J., Magonov S., Thornton J., Ge L., Surface Engineering, 15(4) (1999) 285-290.

[18] S. M. Sze, Physics of Semiconductor Devices, 2nd Ed., J. Wiley and Sons, New York (1981).